npj | precision oncology

Article

Published in partnership with The Hormel Institute, University of Minnesota

https://doi.org/10.1038/s41698-024-00751-2

LSD1 deficiency in breast cancer cells promotes the formation of pre-metastatic niches

Yutong Yao[1], Rui Qian[1], Hanwei Gao[1], Yonghao Dai[1], Yueru Shi[1], Peipei An[1], Benkai Xin[1], Ziyu Liu[1], Nan Zhang[2], Youzhong Wan[1], Yuquan He[2] & Xin Hu[2] ✉

Lysine-specific demethylase 1 (LSD1), a histone demethylating enzyme, plays a crucial role in cancer metastasis. Studies show LSD1 knockout promotes breast cancer lung metastasis, but it's unknown if it alters the lung microenvironment for metastasis. In this study, we investigated the effects of exosomes from LSD1-knockdown (LSD1 KD) breast cancer cells on pre-metastatic niche formation. Injecting exosomes from LSD1 KD cells in mice resulted in a substantial increase in lung colonization by breast cancer cells, while treatment with exosomes derived from LSD1 KD cells decreased the expression of the ZO-1 and occludin, leading to increased vascular permeability. The LSD1 KD reduced the expression of circDOCK1, which augmented the levels of miR-1270 in exosomes. And miR-1270 inhibited ZO-1 expression in human endothelial cells, which enhanced their permeability. Our study uncovered a novel mechanism in which the LSD1 promotes the formation of pre-metastatic niches via the regulation of exosomal miRNA.

Breast cancer is one of the most common tumors worldwide and a leading cause of disability and mortality among women[1]. The rapid advancement of breast cancer treatments has resulted in significant clinical improvements being achieved[2]. However, metastasis remains the primary cause of death for patients with breast cancer, and is associated with a median overall survival period of only 2–3 years[3]. Accordingly, the ability to predict metastasis is crucial for improving patient survival rates. The most common sites for the local metastasis of breast cancer are the lymph nodes, while the most common distant metastatic sites are the lungs, brain, and liver[4].

Metastasis refers to the spreading of tumor cells from primary to distant sites[5]. During this process, tumor cells traverse the compromised vascular wall and enter the bloodstream, becoming circulating tumor cells that disseminate to other parts of the body. Subsequently, they adhere to endothelial cells lining the blood vessels and penetrate adjacent tissues through defective endothelial connections[6].

Whether tumor cells can establish colonization at distant sites largely depends on the formation of pre-metastatic niches (PMNs), microenvironments that facilitate tumor cell colonization[7]. Exosomes as well as other factors derived from tumors both play crucial roles in the formation of pre-metastatic niches[8,9]. Angiogenesis is an essential step in tumor progression and is required for invasive tumor growth and distant metastasis[8,9]. The initial stages of pre-metastatic niche formation are characterized by increased vascular permeability[10]. However, the mechanisms regulating the establishment of pre-metastatic niches are complex and tumor type-specific[11–14].

Exosomes are vesicles with a diameter of ~40–160 nm that are secreted by various types of cells[15]. Cancer-derived exosomes play a crucial role in intercellular communication among tumor cells by transferring oncogenic molecules, including circular RNAs (circRNAs), microRNAs (miRNAs), and proteins, which are involved in tumor initiation, development, angiogenesis, immune evasion, and drug resistance[16–18]. MiRNAs are endogenous, non-coding, single-stranded RNAs ~22–25 nucleotides long[19]. They regulate a wide variety of biological processes, such as cancer progression, remodeling of tumor microenvironments, and formation of pre-metastatic niches, by specifically binding to the 3′-untranslated regions (3′-UTRs) of target genes and inhibiting their expression[20–23]. CircRNAs are members of the non-protein coding RNA family characterized by a closed-loop structure lacking 5′ and 3′ ends[24–26]. They are closely associated with the occurrence and progression of various types of cancers, including breast cancer[27,28]. CircRNAs can regulate gene expression by binding to miRNAs, effectively acting as miRNA sponges[29,30].

Lysine-specific demethylase 1 (LSD1) is a protein that mediates the demethylation of lysine residues in histone H3K4 and H3K9[31]. LSD1

[1]Cancer Biology Laboratory, China-Japan Union Hospital of Jilin University, Jilin University, Changchun, Jilin, China.
[2]Department of Cardiology, China-Japan Union Hospital of Jilin University, Jilin University, Changchun, Jilin, China.
✉e-mail: huxin@jlu.edu.cn

THE HORMEL INSTITUTE
UNIVERSITY OF MINNESOTA

plays an important role in regulating breast cancer growth, invasion, and metastasis[32,33]. The specific effects of LSD1 on breast cancer cells depend on the protein complexes with which LSD1 is associated, as well as the cell type and cell differentiation state[34–39]. We previously showed that the loss of LSD1 in luminal breast cells leads to increased breast cancer lung metastasis in mice, and that the cancer-associated R251Q mutation in LSD1 promotes the progression of luminal breast cancer by disrupting the formation of functional LSD1/CoREST/HDAC complexes[40]. Recently, we also found that exosomes derived from LSD1-knockdown (LSD1 KD) breast cancer cells can activate osteoclastogenesis and inhibit osteoblastogenesis[41,42]. However, it remains unclear whether LSD1 deficiency can promote lung metastasis of breast cancer cells through exosomes.

In this study, we found that exosomes from LSD1 KD breast cancer cells disrupted the lung vascular endothelial barrier by reducing the number of tight junctions in vascular endothelial cells, thereby leading to the formation of pre-metastatic niches in the lung. Mechanistically, LSD1 deficiency reduced the levels of circDOCK1, leading to increased activity of exosomal miR-1270 and the consequent inhibition of the expression of the tight junction proteins ZO-1 and occludin in endothelial cells.

Results

Exosomes from LSD1 KD cells promoted lung colonization of breast cancer cells

To investigate the role of LSD1 in the regulation of breast cancer cell lung metastasis, we transfected MCF7 cells, a luminal breast cancer cell line, with LSD1 shRNA to knockdown LSD1 (LSD1 KD), and subsequently transfected the LSD1 KD cells with a construct resistant to the LSD1 shRNA to rescue LSD1 expression (Rescue). Western blot and qRT-PCR analysis confirmed that the expression of LSD1 was reduced in LSD1 KD cells and was restored in Rescue cells (Fig. 1a, b). Exosomes were isolated from the conditioned media of Control, LSD1 KD, and Rescue cells. The exosomes were enriched with the exosomal markers CD63 and TSG101 (Fig. 1c) and exhibited cup-shaped bilayered membranes (Fig. 1d). Nanoparticle tracking analysis (NTA) revealed that the exosomes were ~132 nm in size and their concentration was $\sim 1 \times 10^7$ particles/mL (Fig. 1e). Furthermore, DiR-labeled exosomes from Control, LSD1 KD, and Rescue cells were intravenously administered to female BALB/c nude mice, and the animals were subsequently subjected to in vivo imaging 24 h, 48 h and 72 h post-injection (Supplementary Fig. 1a), followed by the ex vivo imaging of organs (Supplementary Fig. 1b). The results demonstrated that the exosomes were distributed into multiple organs, including lungs, liver, and brain. Notably, exosomes still present in the lungs of mice at 48 h after exosomes were injected into the body, while at 72 h, exosomes disappeared from the lungs mostly (Supplementary Fig. 1b). Consequently, to maintain a continuous presence of exosomes in the lungs, we chose a frequency of injections every 3 days.

To investigate the effects of exosomes from LSD1 KD cells on breast cancer cell lung colonization, mice were treated with exosomes from the three cell lines via tail vein injection, and fluorescently labeled MCF7 cells were subsequently infused into these mice through intracardiac injection (Fig. 1f). After 6 weeks, bioluminescence imaging was performed to determine whether the MCF7 cells colonized the lungs. Mice treated with exosomes from LSD1 KD cells showed significantly higher lung colonization than mice treated with exosomes from Control or Rescue cells (Fig. 1g–i). Consistently, immunohistochemistry (IHC) staining showed that Ki67 staining was more extensive in the lungs of mice treated with exosomes from LSD1 KD cells than in the lungs of mice treated with exosomes from Control or Rescue cells (Fig. 1j). Similarly, exosomes from LSD1 KD cells also promoted lung colonization of fluorescently labeled MDA-MB-231 cells, a triple negative breast cancer cell line (Supplementary Fig. 2a–e). Taken together, our results demonstrated that exosomes from LSD1 KD cells promoted breast cancer cell lung colonization.

Exosomes from LSD1 KD cells enhanced vascular permeability

To investigate whether the promotion of breast cancer cell lung colonization by exosomes from LSD1 KD cells involved the enhancement of vascular permeability, we injected exosomes from Control, LSD1 KD, and Rescue cells into the tail veins of female BALB/c nude mice and then examined the organs frequently affected by breast cancer metastasis, such as lung and brain (Fig. 2a). Immunofluorescence assays demonstrated that exosomes from LSD1 KD cells decreased the expression of ZO-1 and occludin in lung endothelial cells that were positive for cluster of differentiation 31 (CD31) staining (Fig. 2b, c). Similarly, the expression of these two tight junction proteins was also decreased in CD31-positive endothelial cells in the brains of mice treated with exosomes from LSD1 KD cells (Fig. 2d, e). Because ZO-1 and occludin play important roles in the maintenance of tight junctions that seal endothelial cells[12,43], the decreased expression of these two proteins in vascular endothelial cells suggested that breast cancer cells were more likely to invade through this disrupted vascular endothelial barrier. To confirm these effects of exosomes from LSD1 KD cells on vascular permeability, rhodamine B isothiocyanate-dextran was injected into mice after exosome treatment. Animals treated with exosomes from LSD1 KD cells showed increased rhodamine leakage in the lungs and liver, indicating increased vascular permeability (Fig. 2f–h).

Exosomes from LSD1 KD cells disrupted barrier function of endothelial monolayer

Next, we investigated the function of exosomes from LSD1 KD cells in vitro. PKH67-labeled exosomes were cultured together with endothelial cells, HPMECs and HUVECs, and fluorescence staining demonstrated that these exosomes could be absorbed by endothelial cells, and were mostly localized to the cytoplasm (Fig. 3a, b). Treatment with exosomes from LSD1 KD cells resulted in a significant decrease in the protein expression of ZO-1 and occludin in endothelial cells (Fig. 3c, d). Similarly, immunofluorescence staining assays showed that endothelial cell treated with exosomes from LSD1 KD cells exhibited a marked reduction in ZO-1 levels as well as tight junction disruption (Supplementary Fig. 3a, b).

We next conducted an in vitro permeability assay by measuring the amount of rhodamine-labeled dextran traversing an endothelial cell monolayer. Treatment of the endothelial monolayer with exosomes from LSD1 KD cells increased the amount of rhodamine-labeled dextran crossing from the top to bottom chambers of the Transwell filters, indicative of increased endothelial monolayer permeability (Fig. 3e, f). In line with this result, treatment with exosomes from LSD1 KD cells significantly reduced the resistance per unit area of endothelial monolayers in TEER experiments (Fig. 3g, h). Importantly, the number of GFP-labeled MCF7 cells invading through the endothelial monolayer treated with exosomes from LSD1 KD cells was significantly higher than the number of cells invading through the endothelial monolayer treated with exosomes from Control or Rescue cells (Fig. 3i, j). Similarly, exosomes from LSD1 KD cells also promoted GFP-labeled MDA-MB-231 invading through the endothelial monolayer. (Supplementary Fig. 3c, d). Together, these results demonstrated that exosomes from LSD1 KD cells disrupted the barrier function of endothelial monolayers.

LSD1 knockdown affected the expression of miRNAs in exosomes

To understand how the knockdown of LSD1 in breast cancer cells affects exosomal miRNA levels, we analyzed exosomal miRNA contents using whole transcriptome sequencing. LSD1 expression was confirmed to be altered in both LSD1 KD and Rescue cells (Fig. 4a). Differentially expressed miRNAs were selected using a fold change (FC) ≥ 2 and a p-value < 0.05 as thresholds. A total of 325 miRNAs displayed differential expression between exosomes from Control cells and those from LSD1 KD cells, while 1212 miRNAs were differentially

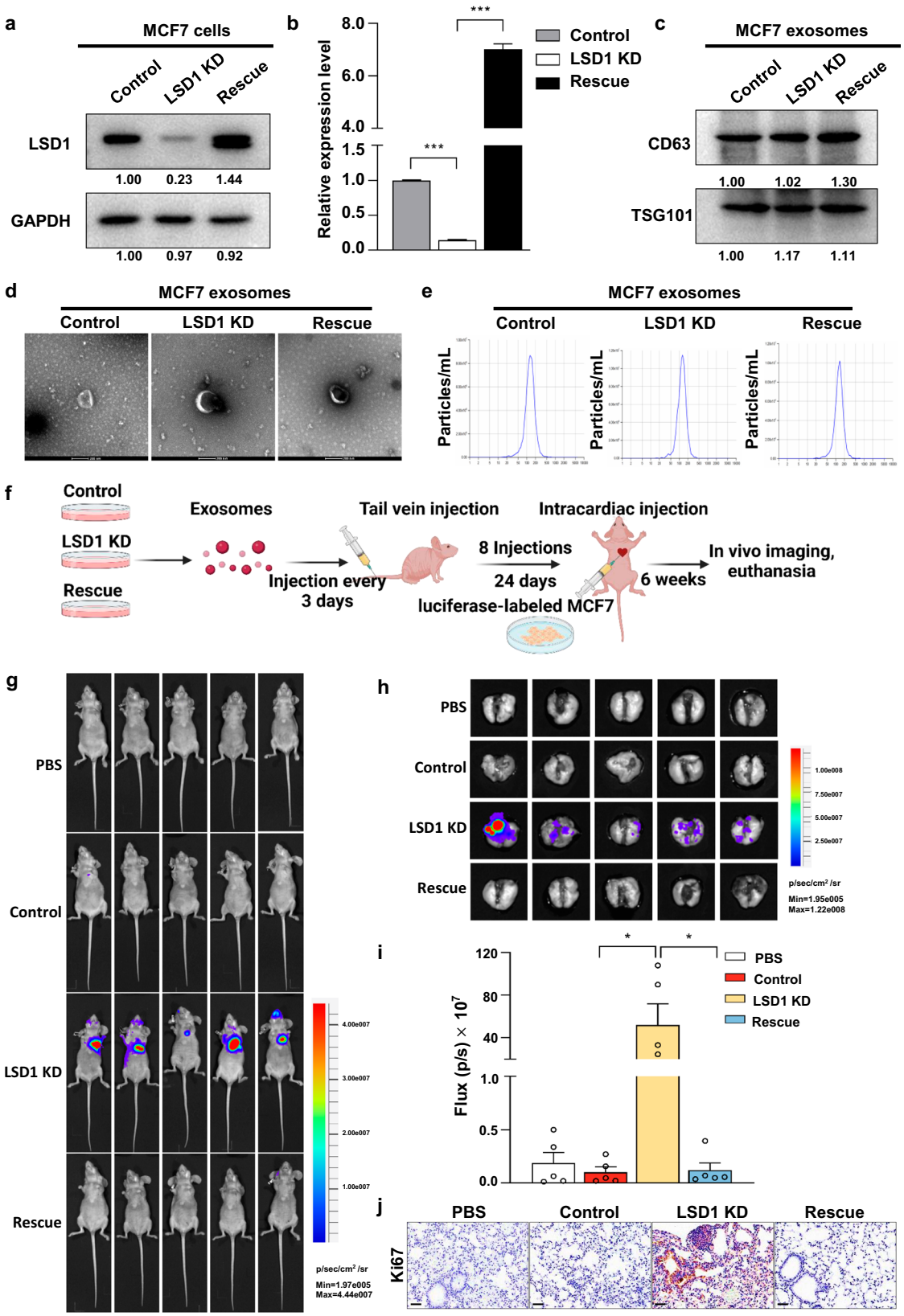

expressed between exosomes from LSD1 KD cells and those from Rescue cells; among these miRNAs, 195 showed differential expression in both comparisons (Fig. 4b).

Among the 195 overlapping differentially expressed miRNAs, 99 were upregulated in exosomes from LSD1 KD cells and reversed in exosomes from Rescue cells (Fig. 4b). As these 99 miRNAs were more likely to be involved in LSD1-mediated metastasis of breast cancer cells, we focused on these miRNAs in subsequent studies (Fig. 4c). qRT-PCR analysis confirmed the sequencing results for some of the 99 exosomal miRNAs, including miR-1270, miR-4800-3p, and miR-1290 (Fig. 4d).

Fig. 1 | Exosomes from LSD1 knockdown cells promote lung colonization of MCF7. a Western blot analysis of LSD1 expression in MCF7 cells transfected with the control construct (Control), MCF7 cells transfected with LSD1 shRNA (LSD1 KD), and LSD1 KD MCF7 cells in which LSD1 expression is restored (Rescue). **b** qRT-PCR analysis of LSD1 expression in Control, LSD1 KD, and Rescue cells. Data are presented as means ± SEM ($n = 3$). ***$p < 0.001$. **c** Western blot analysis of the exosomal markers CD63 and TSG101 in purified exosomes from Control, LSD1 KD, and Rescue cells. **d** Transmission electron micrographs of exosomes from Control, LSD1 KD, and Rescue cells. Scale bars: 100 nm. **e** Nanoparticle tracking analysis (NTA) of the diameter and concentration of exosomes from Control, LSD1 KD, and Rescue cells. **f** Schematic representation (created with BioRender.com) of exosome injection via tail vein and the intracardiac injection of luciferase-labeled MCF7 cells into BALB/c-nu/nu mice. **g, h** Bioluminescence imaging of the whole body and lungs of mice injected with luciferase-labeled MCF7 cells and treated with the indicated exosomes. **i** The tumor burden in lungs was quantified by measuring the total flux (photons/s) in bioluminescence imaging. Data are presented as means ± SEM ($n = 5$). *$p < 0.05$. **j** Immunohistochemical (IHC) staining for Ki67 in lung sections from mice treated with the indicated exosomes.

MiR-1270 mediated the effects of exosomes from LSD1 KD cells on the barrier function of endothelial monolayers by decreasing ZO-1 expression

The transfection of miR-1270 led to an increase in the amount of fluorescence probe that crossed endothelial monolayers, indicating that the permeability of these endothelial monolayers was increased. However, the transfection of miR-4800-3p and miR-1290 mimics had no effect on endothelial permeability (Supplementary Fig. 4a and Fig. 5a, b). Consistent with these observations, significant decreases in trans-endothelial resistance were recorded in endothelial monolayers following treatment with miR-1270 mimics. miR-4800-3p or miR-1290 mimics did not affect endothelial resistance (Supplementary Fig. 4b and Fig. 5c, d).

The number of GFP-labeled MCF7 cells invading through endothelial cell transfected with miR-1270 mimics was also significantly increased (Fig. 5e, f and Supplementary Fig. 5a, b). The same results were obtained in GFP-labeled MDA-MB-231 (Supplementary Fig. 5c, d). We transfected mimic-1270 into MCF7 cells and inhibitor-1270 into LSD1 KD cells, and isolated exosomes from the transfected cells to treat endothelial cells. When MCF7 cells were transfected with mimics1270, miR-1270 levels in exosomes were also increased (Supplementary Fig. 6a). Consistently, when MCF7 cells were transfected with inhibitor-1270, the levels of miR-1270 in exosomes were decreased (Supplementary Fig. 6a). HUVEC cells treated with exosomes from mimics-1270 transfected MCF7 cells showed a significant reduction in ZO-1 expression, while transfection of inhibitor-1270 into LSD1 KD cells effectively reversed the decreased expression of ZO-1 in HUVEC treated with exosomes from the LSD1 KD cells (Supplementary Fig. 6b). Together, these results demonstrated that miR-1270 mediated the effects of exosomes derived from LSD1 KD cells on the barrier function of endothelial monolayers.

MiRDB, miRWalk, Targetscan, and mirDIP databases were used to analyze the potential target genes of miR-1270, leading to the identification of a total of 162 genes from all these 4 databases (Fig. 5g). KEGG pathway enrichment analysis revealed that these 162 genes were enriched in gap junction, tight junction, and adherens junction pathways (Fig. 5h). Similarly, GO term enrichment analysis indicated that these 162 target genes were enriched in pathways involved in positive regulation of cell adhesion, cell-cell adhesion mediated by calcium-binding proteins, and cell-cell junctions (Supplementary Fig. 7a). Notably, ZO-1 was predicted to be a target gene of miR-1270, and its expression was indeed reduced in HPMECs and HUVECs transfected with miR-1270 mimics (Fig. 5i, j and Supplementary Fig. 7b). To investigate how miR-1270 regulates ZO-1 expression, we mutated the potential binding sites of miR-1270 in the 3′-UTR of ZO-1 and cloned the wild-type and mutated 3′-UTRs into the luciferase reporter vector, pmirGLO. We found that miR-1270 significantly reduced the luciferase activity of the pmirGLO-ZO-1-WT construct, while it had no effect on the luciferase activity of the pmirGLO-ZO-1-MUT construct (Fig. 5k). In summary, our results demonstrated that miR-1270 disrupted the barrier function of endothelial cell monolayers by downregulating ZO-1 expression.

CircDOCK1 expression was significantly downregulated in LSD1 KD cells

To examine the mechanism underlying how LSD1 regulates exosomal miR-1270, we sought to identify which cellular circRNAs were affected by LSD1 knockdown using whole transcriptome sequencing. Differentially expressed circRNAs were selected based on a fold change (FC) ≥ 2 and a p-value < 0.05. A total of 57 circRNAs showed differential expression between Control and LSD1 KD cells, while 56 showed differential expression between LSD1 KD cells and Rescue cells; 18 circRNAs exhibited differential expression in both comparisons (Fig. 6a). Among these 18 circRNAs, 14 were downregulated in LSD1 KD cells and concomitantly upregulated in Rescue cells, while 4 circRNAs displayed the opposite trend (Fig. 6b). Considering that the 14 circRNAs that were downregulated in LSD1 KD cells were likely to be involved in regulating exosomal miR-1270 expression, we selected those with the highest expression levels for validation by qRT-PCR, which showed that the expression of circDOCK1 (circ0020397) and circSEMA3C (circ0004365) was decreased in LSD1 KD cells (Fig. 6c). CircRNAs can function as miRNA sponges, sequestering them and inhibiting their function[44]. Therefore, we identified which miRNAs were likely to be sponged by circDOCK1 using the online databases circBank and Circinteractome. A total of 13 miRNAs were identified as potential targets of circDOCK1 by both databases[45]. By intersecting with the 99 upregulated miRNAs identified in exosomes from LSD1 KD cells, we identified three miRNAs that could potentially be sponged by circDOCK1, namely, miR-1270, miR-1265, and miR-1246 (Fig. 6d, e).

Divergent and convergent primers were designed to amplify the circular and linear transcripts of DOCK1, respectively, and RT-PCR results confirmed that circDOCK1 was resistant to digestion by RNase R (Fig. 6f, g). Subsequently, we designed primers to specifically amplify the junction site of circ0020397 (circDOCK1) and subjected the PCR products to Sanger sequencing (Fig. 6h). To determine the cellular localization of circDOCK1, qRT-PCR analysis was performed on nucleus and cytoplasm of MCF7 cells, demonstrating that circDOCK1 was predominantly localized to the cytoplasm (Fig. 6i). Fluorescence in situ hybridization (FISH) analysis also confirmed the cytoplasmic localization of circDOCK1 (Fig. 6j). These findings suggested that circDOCK1 might function as a sponge for miR-1270, thereby influencing the expression of miR-1270 in exosomes.

CircDOCK1 suppressed the expression of exosomal miR-1270

To investigate whether circDOCK1 could indeed sequester miR-1270, we designed siRNAs targeting the reverse splicing site of circDOCK1 (Fig. 7a). qRT-PCR analysis confirmed that the expression of circDOCK1 was significantly decreased in MCF7 cells transfected with these siRNAs (Fig. 7b) and that the expression of miR-1270 was significantly increased in MCF7 cells transfected with circDOCK1 siRNA (Fig. 7c). Importantly, the expression of miR-1270 in exosomes derived from MCF7 cells transfected with circDOCK1 siRNA also showed a significant increase (Fig. 7c). In line with this finding, the overexpression of circDOCK1 led to a significant decrease in cellular and exosomal miR-1270 expression in MCF7 cells (Fig. 7d, e). Furthermore, RNA pulldown experiments showed a significant enrichment of miR-1270 when the circDOCK1 probe was used (Fig. 7f, g). Similarly, a reverse pulldown experiment showed that circDOCK1 was significantly enriched when a miR-1270 probe was employed (Fig. 7h). Together, these results confirmed the interactions between circDOCK1 and miR-1270. Furthermore, the binding sites between circDOCK1 and miR-1270 were predicted using the online bioinformatics database Circinteractome (Fig. 7i). Co-transfection of miR-1270 mimics and wild-type circDOCK1 (circDOCK1 WT) into HEK293T cells led to a significant

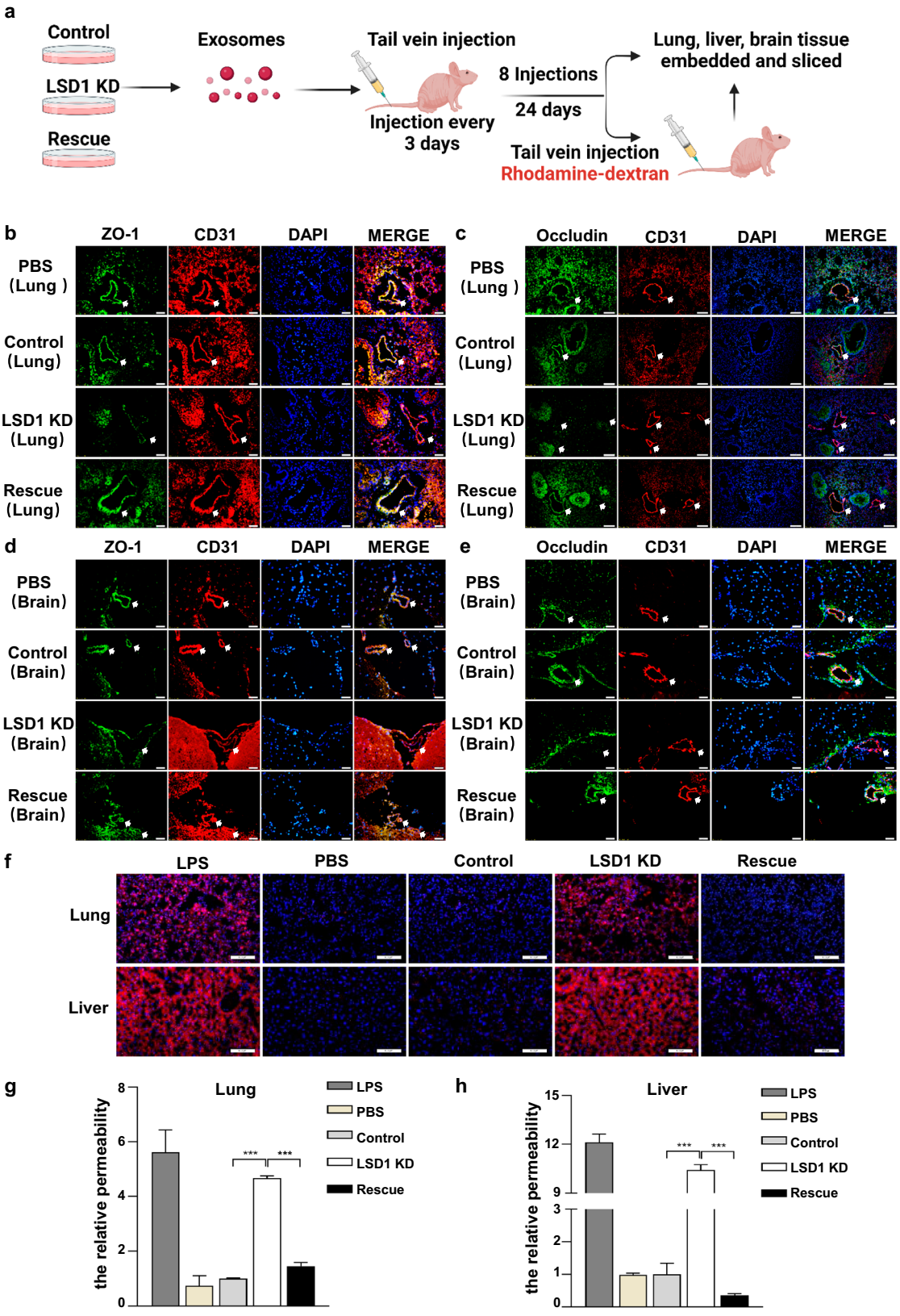

Fig. 2 | Exosomes from LSD1 knockdown cells increase vascular permeability. **a** Schematic representation (created with BioRender.com) of the administration of the indicated exosomes and rhodamine-dextran via tail vein injection. **b**–**e** Immunofluorescence (IF) staining of lung (**b**, **c**) and brain (**d**, **e**) sections for ZO-1 (**b**, **d**) and occludin (**c**, **e**). CD31 (red) and nuclei (blue) are also stained. Tissues positive for CD31 are indicated by arrowheads. Scale bars: 20 μm. **f** IF analysis of rhodamine-dextran (red) in lung and liver sections of mice treated with the indicated exosomes. Nuclei are stained with DAPI (blue). LPS, Lipopolysaccharide. Scale bars: 100 μm. **g**, **h** Quantification of rhodamine in the lungs and liver ($n = 3$). Data are presented as means ± SEM. $^{***}p < 0.001$.

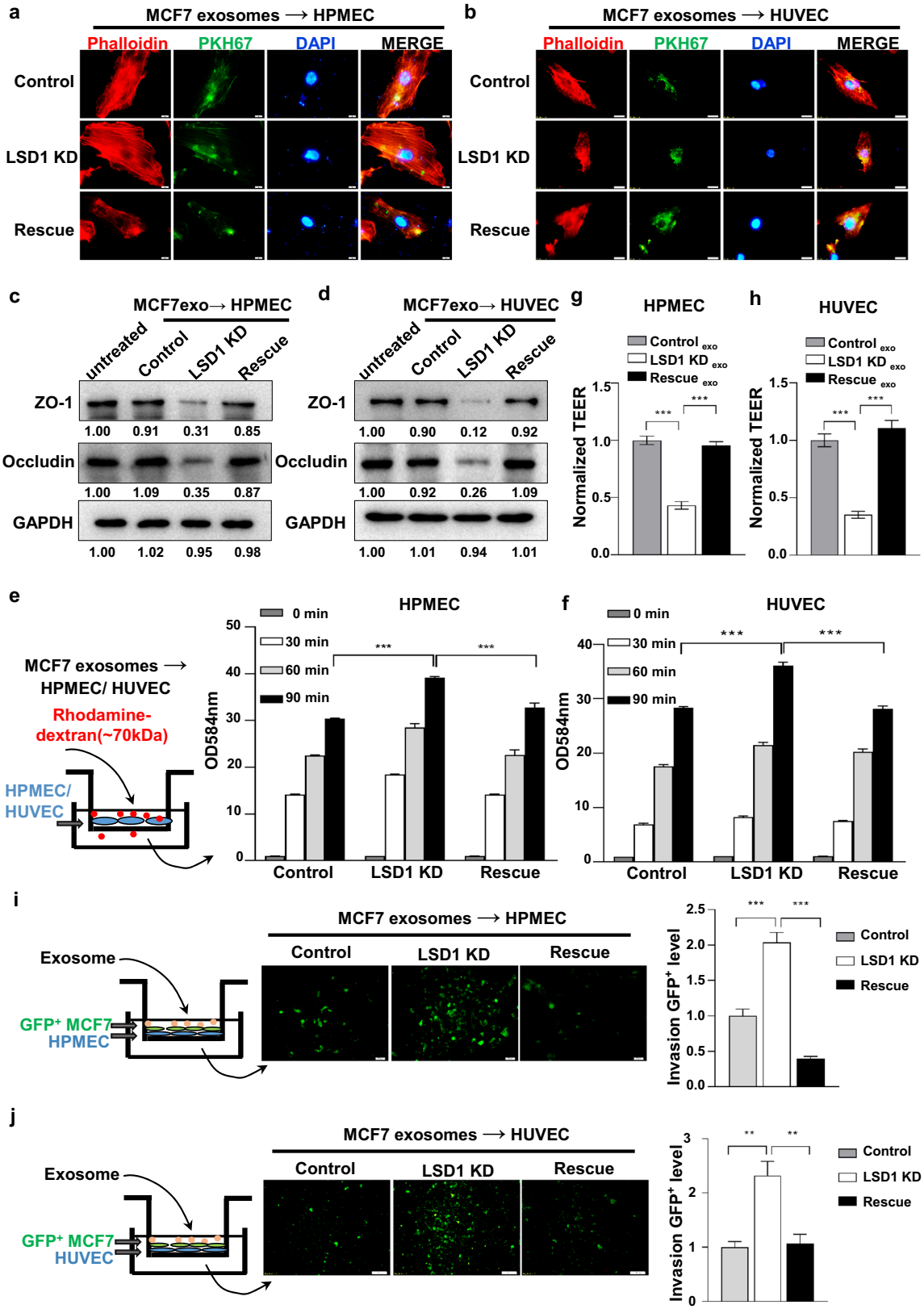

Fig. 3 | Exosomes from LSD1 knockdown cells disrupt barrier function in endothelial cells. a, **b** Immunofluorescence (IF) analysis of human lung microvascular endothelial cells (HPMECs) **a** and human umbilical vein endothelial cells (HUVECs) **b** incubated with PKH67-labeled exosomes (green). Scale bars: 10 μm. **c**, **d** Western blotting analysis of ZO-1 and occludin expression in HPMECs and HUVECs treated with the indicated exosomes. **e**, **f** Transwell assays for the determination of the amount of rhodamine-dextran that passes through monolayers formed by HPMECs ($n = 4$) and HUVECs ($n = 3$) treated with the indicated exosomes. **g**, **h** Analysis of trans-endothelial electrical resistance (TEER) in monolayers formed by HPMECs ($n = 6$) and HUVECs ($n = 4$) treated with the indicated exosomes. **i**, **j** Transwell assays for the determination of the number of GFP-labeled MCF7 cells that pass through monolayers formed by HPMECs ($n = 5$) and HUVECs ($n = 5$) treated with the indicated exosomes, with quantification of the numbers of invading MCF7 cells. Scale bars: 50 μm.

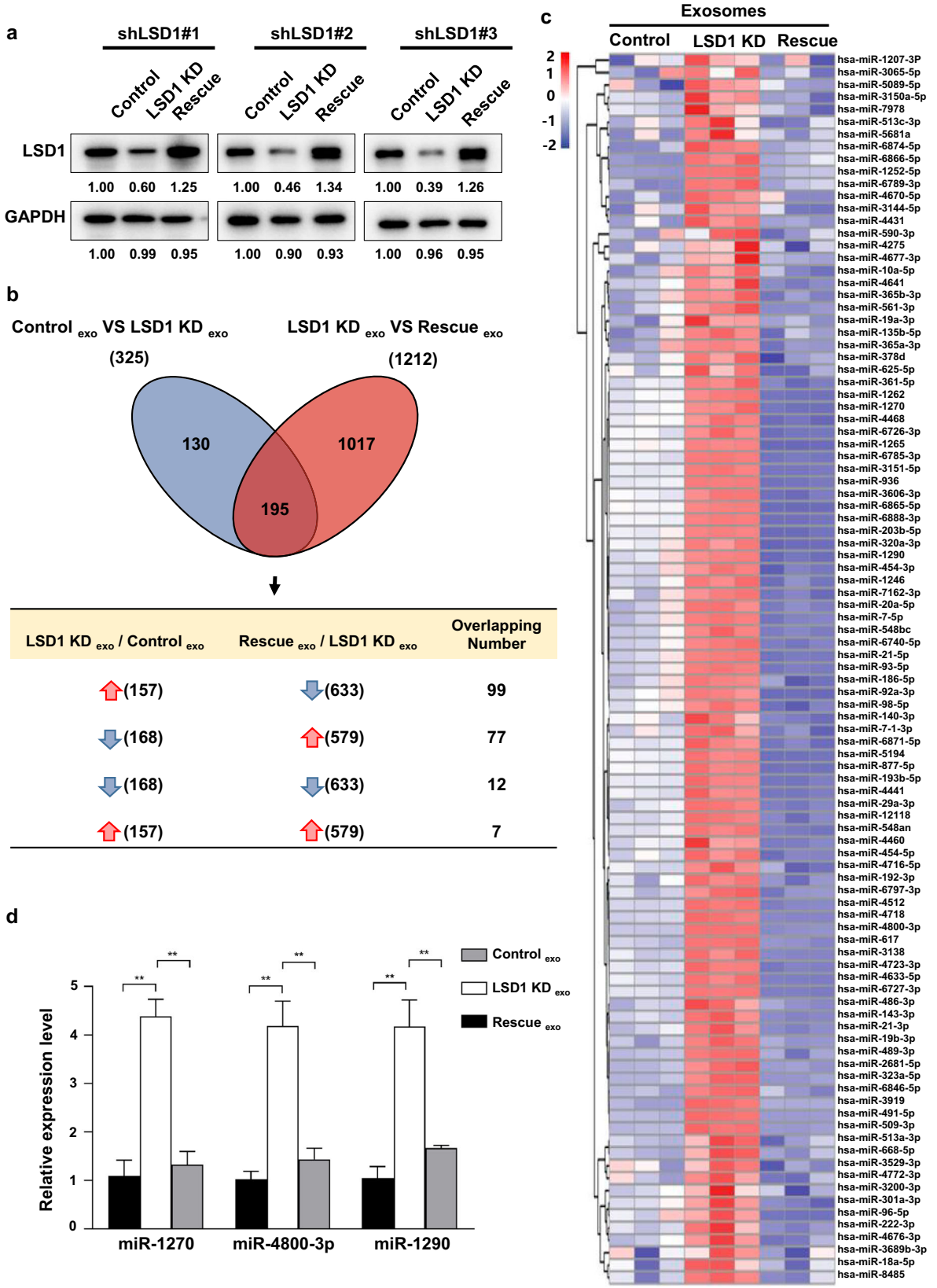

Fig. 4 | LSD1 knockdown alters the expression of exosomal miRNAs in MCF7 cells. a Western blot analysis of LSD1 expression in Control, LSD1 knockdown (KD), and Rescue cells in three independent batches of samples. **b** Venn diagram showing the number of differentially expressed miRNAs between Control and LSD1 KD exosomes and between LSD1 KD and Rescue exosomes. **c** Heat map of the exosomal miRNAs that are significantly upregulated in LSD1 KD exosomes and restored in Rescue exosomes. **d** qRT-PCR analysis of the expression levels of the indicated miRNAs in Control, LSD1 KD, and Rescue exosomes. Data are presented as means ± SEM ($n = 3$ unless otherwise indicated). $^{*}p < 0.05$, $^{**}p < 0.01$.

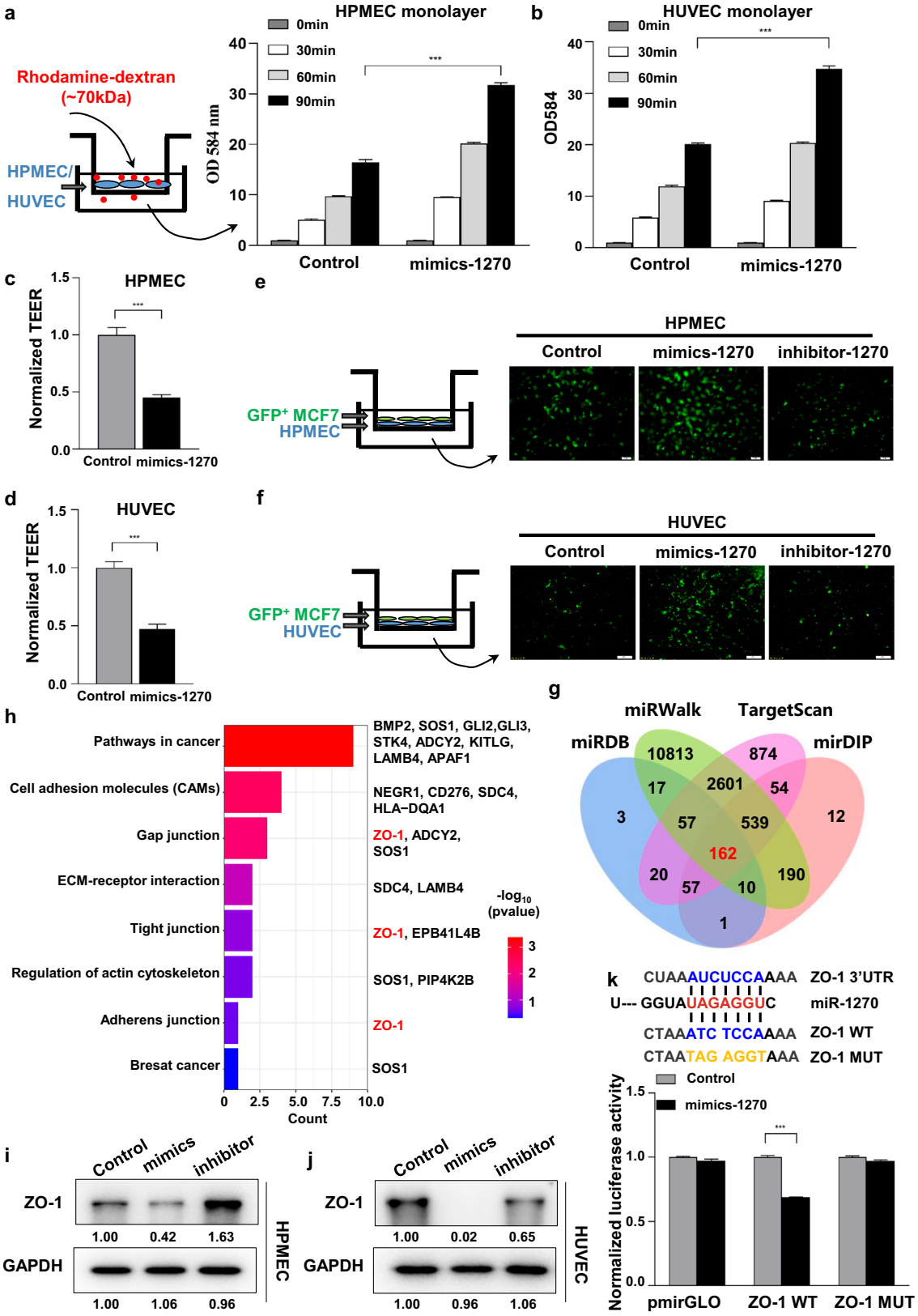

decrease in luciferase activity compared with co-transfection of miR-NC and circDOCK1-WT (Fig. 7i). Furthermore, FISH analysis further confirmed the colocalization of circDOCK1 and miR-1270 in cells (Fig. 7j). In summary, these results demonstrated that circDOCK1 can act as a sponge for miR-1270.

Discussion

Exosomes are important mediators of cell communication. Tumor-derived exosomes can mediate the crosstalk between tumors and distant organs, altering the microenvironment of the latter, and thereby facilitating the formation of a pre-metastatic niche and, consequently,

Fig. 5 | MiR-1270 disrupts the barrier function of endothelial monolayers by decreasing the expression of ZO-1. a, **b** Transwell assays for the amount of rhodamine-dextran that passes through monolayers formed by HPMECs and HUVECs transfected with Control or miR-1270 mimics. **c**, **d** Analysis of trans-endothelial electrical resistance (TEER) in HPMECs ($n = 6$) and HUVECs ($n = 9$) transfected with Control or miR-1270 mimics. **e**, **f** Transwell assays for the numbers of GFP-labeled MCF7 cells that pass through monolayers formed by HPMECs and HUVECs transfected with Control, miR-1270 mimics, or miR-1270 inhibitor. Scale bars: 50 μm. **g** Venn diagram showing the number of miR-1270 target genes predicted by TargetScan, miRDB, miRWalk, and mirDIP. **h** KEGG pathway analysis of the 162 miR-1270 target genes predicted by the four databases. **i**, **j** Western blot analysis of ZO-1 expression in HPMECs and HUVECs transfected with Control, miR-1270 mimics, or miR-1270 inhibitor. **k** The sequences of the predicted miR-1270 binding sites in the 3′-UTR of ZO-1. Firefly luciferase reporter plasmids containing wild-type (ZO-1 WT) or mutant (ZO-1 MUT) binding sites for miR-1270 were co-transfected with miR-1270 mimics or into HEK293T cells, and the relative luciferase activities were analyzed. Data are presented as means ± SEM ($n = 3$ unless otherwise indicated). $^{***}p < 0.001$.

promoting tumor metastasis[46]. In our previous study, we demonstrated that the knockout of LSD1 markedly enhances lung metastasis of breast cancer[47]. Here, we found that exosomes from LSD1 KD breast cancer cells could promote breast cancer cell lung colonization. The knockdown of LSD1 decreased the expression of circDOCK1, leading to reduced miR-1270 sequestration by circDOCK1, which enhanced the levels of miR-1270 in exosomes. MiR-1270 inhibited the expression of ZO-1 in vascular endothelial cells at distant organs, resulting in tight junction disruption in these cells alongside enhanced vascular permeability (Fig. 8). Such remodeling of the microenvironment at distant organs promoted the establishment of pre-metastatic niches for breast cancer metastasis.

Exosomal miRNAs play a crucial role in promoting the formation of pre-metastatic niches in breast cancer. Given that they are protected from degradation in the bloodstream, exosomal miRNAs can be efficiently delivered to distant organs[48]. Breast cancer cells with high metastatic ability overexpress miR-105, which disrupts the tight connections between endothelial cells by reducing the expression of ZO-1, thus enhancing cancer cell metastasis to the lungs[12]. One study showed that miR-939 from breast cancer cell-derived exosomes can be absorbed by endothelial cells in blood vessels, leading to a reduction in VE-cadherin expression and the disruption of the connections among endothelial cells, which enhanced vascular permeability, thus facilitating cancer cell migration through blood vessels and promoting metastasis[49]. In our study, we found that miR-1270 also disrupted tight junctions among endothelial cells, resulting in enhanced vascular permeability. MiR-21-5p expression is markedly increased in colorectal cancer, and exosomal miR-21-5p was reported to increase vascular permeability by targeting KRIT1[50]. Here, we identified miR-1270 as a novel player in breast cancer, regulating angiogenesis and vascular permeability. Through in vitro experiments, we confirmed that miR-1270 can reduce trans-endothelial resistance, enhance endothelial cell permeability, and promote the formation of vascular-like structures in HUVECs. Further analysis of the function of miR-1270 alongside target gene prediction revealed that this miRNA enhances vascular permeability and promotes the formation of pre-metastatic niches by inhibiting ZO-1 expression. This represents a novel mechanism through which miR-1270 enhances lung metastasis of breast cancer cells.

CircRNAs can act as competitive endogenous RNAs (ceRNAs) by sequestering miRNAs, thus indirectly regulating their functional effects. Dysregulation of these ceRNA networks can lead to cancer. For example, ciRS-7, a well-characterized circRNA in triple-negative breast cancer, contains binding sites for and sponges miR-1299, thereby upregulating the expression of matrix metalloproteinase family members and augmenting the migratory and invasive characteristics of breast cancer cells[51]. Another example is circEPSTI1, which upregulates the expression of BCL6809A by binding to miR-11 and miR-4753 and thereby promoting breast cancer proliferation and apoptosis[52]. These studies revealed the potential of circRNAs as biomarkers and therapeutic targets in breast cancer diagnosis and treatment. In this study, we identified circDOCK1 as a ceRNA in breast cancer cells. Tellez-Gabriel et al. [53] reported that circDOCK1 regulates IGF1R expression through targeting miR-339-3p, which promotes the occurrence of osteosarcoma and cisplatin resistance. Further research into the functional roles of circRNAs and their interactions with other cellular components will likely elucidate their roles in breast cancer in greater detail.

In summary, our findings demonstrated that the downregulation of LSD1 expression in breast cancer cells altered the expression of circRNAs in these cells. Through sponging, circRNAs altered the expression of miRNAs in extracellular vesicles, some of which contribute to the reshaping of pre-metastatic niches, thereby creating a favorable microenvironment for breast cancer cell metastasis. Our findings further highlighted the significant role played by epigenetic modifications in the regulation of exosomal miRNAs and their crucial involvement in breast cancer metastasis.

Methods

Ethical approval

All animal experiments were conducted according to the Guide for the Care and Use of Laboratory Animals of the National Institutes of Health and were approved by the Animal Ethics Committee of the Changchun Wish Technology Company (IACUC Issue No. 20220923-01 and IACUC Issue No. 20240220-01).

Cell lines, cell culture, and transfection

The human breast cancer cell lines MDA-MB-231 and MCF7, human lung microvascular endothelial cells (HPMECs), human umbilical vascular endothelial cells (HUVECs), and human embryonic kidney (HEK) 293T cells were purchased from ATCC and were cultured in-house. MDA-MB-231 and MCF7 cells were cultured in Dulbecco's Modified Eagle's Medium (DMEM; Gibco, Australia) while HUVECs were cultured in Endothelial Cell Medium (ECM; ScienCell, USA). Both media were supplemented with 10% fetal bovine serum (FBS; BI, Israel) and 1% penicillin/streptomycin (Solarbio, China). Additionally, 0.5 μg/mL puromycin (Solarbio), 1 μg/mL G418 (Gentihold, China), and 1% endothelial cell growth supplement were added as needed. All cells were maintained at 37 °C in a humidified environment with 5% CO_2. Lentiviruses were generated by co-transfecting HEK293T cells using the packaging system. Culture supernatants were collected, concentrated, titrated, and used for cellular transduction. Puromycin and G418 were used for the selection of cells stably expressing the lentiviral constructs. MiR-1270 mimics and miR-1270 inhibitor were purchased from GenePharma (Suzhou, China). Transfection was carried out using RNAiMAX (Invitrogen, USA) following the manufacturer's instructions.

Exosome purification and characterization

MCF7 cells were cultured in DMEM without fetal bovine serum for 36 h. Conditioned medium was collected, centrifuged at 300 × *g* for 10 min, and the resulting supernatant was further centrifuged at 2,000 × *g* for 10 min to remove apoptotic bodies and large cell debris. The conditioned medium was then centrifuged again at 2000 × *g* for 10 min, the supernatant was filtered through a 0.22-μm filter (Millipore, MA, USA), and again centrifuged at 5,000 × *g* to concentrate the exosomes. Total Exosome Isolation Reagent (Invitrogen, NY, USA) was added to the supernatant at half volume and the mixture was incubated overnight at 4 °C. Subsequently, the solution was centrifuged at 10,000 × *g* for 1 h and the precipitate was collected as the isolated exosomes, which were dissolved in PBS at 10 μg/mL for in vitro experiments. The size, morphology, and number of exosomes were

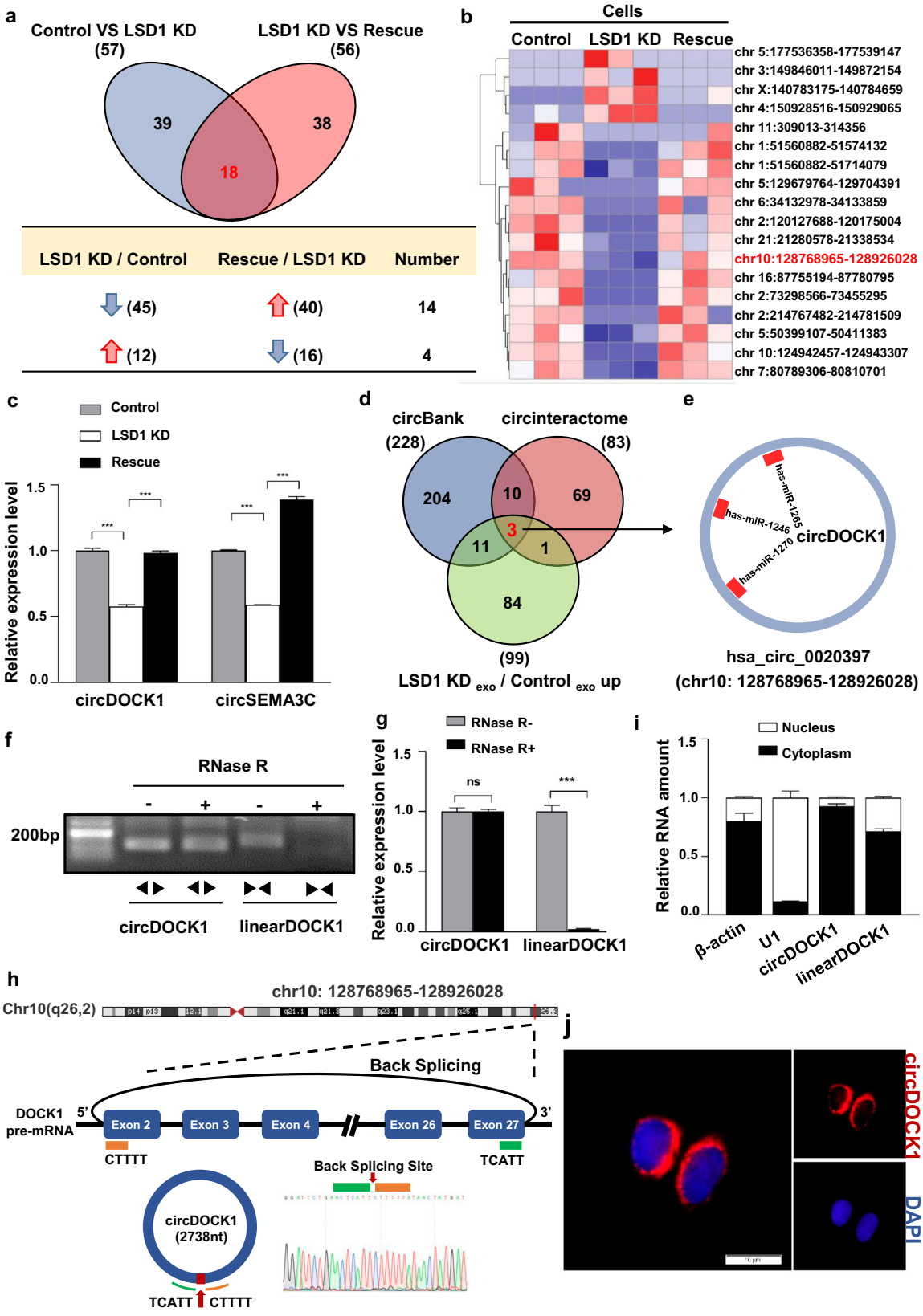

characterized using a ZetaView nanoparticle analyzer (Particle Metrix, DEU) and transmission electron microscopy (TEM) (FEI, Teaj G2 Spirit BigTw, USA) by Shanghai Outdo Biotech Co., Ltd. (Shanghai, China). Western blot was used to analyze the expression of the exosomal biomarker proteins CD63 and TSG101.

Western blotting

Total protein was extracted from whole cells by lysing in RIPA lysis buffer. Equal amounts of protein (10 μg) were separated by 8%–12% SDS–PAGE and electrically transferred to a 0.22-μm PVDF membrane (Millipore). The membrane was blocked with 5% nonfat milk at room temperature for

Fig. 6 | LSD1 knockdown decreases the expression of circRNAs. a Venn diagram showing the number of differentially expressed circRNAs between Control and LSD1 knockdown (KD) cells and between LSD1 KD and Rescue cells. **b** Heat map of the circRNAs that are both significantly changed in LSD1 KD cells and restored in Rescue cells. **c** The relative expression of circDOCK1 and circSEMA3A in Control, LSD1 KD, and Rescue cells ($n = 4$). **d** Venn diagram showing the number of circDOCK1 target miRNAs predicted by circBank and Circinteractome and the number of miRNAs upregulated in LSD1 KD exosomes. **e** Schematic diagram showing the binding sites of miR-1270, miR-1246, and miR-1265 in circDOCK1. **f** PCR analysis of circDOCK1 and its linear isoform DOCK1 after treatment with RNase R. **g** qRT-PCR analysis of circDOCK1 and its linear DOCK1 after treatment with RNase R. **h** Schematic diagram showing the genomic locus of the DOCK1 gene and the back-splicing of circDOCK1. The red arrow indicates the back-splicing site of DOCK1, which was confirmed by Sanger sequencing. **i** qRT-PCR analysis of the nuclear-cytoplasmic fractionation of circDOCK1. **j** Fluorescence in situ hybridization (FISH) analysis of the subcellular localization of circDOCK1 in MCF7 cells. Data are presented as means ± SEM ($n = 3$ unless otherwise indicated). $^{***}p < 0.001$.

30 min, and then incubated at 4 °C overnight with primary antibodies targeting occludin (ABclonal, A2601, 1:1000), ZO-1 (Proteintech, 21773-1-AP, 1:500), LSD1 (Cell Signaling Technology, 2139S, 1:1000), GAPDH (Bioworld, AP0063, 1:2000), CD63 (Abcam, ab59479, 1:1000), and TSG101 (Abcam, ab83, 1:500). The next day, the membrane was incubated with horseradish peroxidase (HRP)-labeled secondary antibody for 1 h at room temperature. Images were captured using the Tanon 5200 Chemiluminescent Imaging System (Tanon Science & Technology, Shanghai, China).

qRT-PCR and RT-PCR

SnRNA U6 was used for the normalization of miRNA levels while β-actin was used for the normalization of circRNA and mRNA expression levels in qRT-PCR. Relative gene expression levels were calculated by the $2^{-\Delta\Delta Ct}$ method. The primer sequences are listed in Supplementary Table 1. PCR products were analyzed using 2% agarose gel electrophoresis (120 V, 30 min) with TAE running buffer. Super DNA Marker was used as the DNA marker (Takara, 3590 A, China). The primer sequences are listed in Supplementary Table 2. All primers were synthesized by Invitrogen (USA).

Animals

Female BALB/c-nu/nu (nude) mice (4-5 weeks old, 16–20 g) were provided by Beijing Vital River Laboratory Animal Technology Co, China. All mice were maintained at Changchun Wish Technology Company under specific pathogen-free conditions and a 12-h/12-h light/dark cycle. The mice were acclimatized and housed for 1 week before the experiment. In the experimental design, in order to control for potential bias, we used randomization and blinding. For the exosome treatment experiment, exosomes were intravenously injected into 5–6-week-old female BALB/c-nu/nu (nude) mice through the tail vein (50 μg of exosomes per injection, one injection every 3 days). After eight injections, the lungs, brain, and liver were harvested, fixed, and paraffin-embedded for subsequent experiments. 1×10^5 luciferase-labeled MCF7 cells or 1×10^6 luciferase-labeled MDA-MB-231 cells were used for intracardiac injection. For exosome tracing experiments, the lipophilic indocyanine dye DiR (Invitrogen, D12731) was added to the exosomes. The DiR-labeled exosomes were then washed twice with PBS to remove excess dye and then injected into female BALB/c nude mice via the tail vein. Intracardiac injections and in vivo imaging in mice were anesthetized by inhalation of oxygen containing 1.5-2.0% isoflurane. After euthanizing the mice with carbon dioxide, individual tissues from each group of mice were collected for subsequent experiments.

Immunohistochemistry and tissue immunofluorescence staining

Tissues were fixed in 4% paraformaldehyde, embedded in paraffin, and sliced into 4-μm-thick transverse sections. For the IHC assay, paraffin-embedded sections were incubated first with an anti-Ki67 antibody (Servicebio, GB111141, 1:500) at 4 °C overnight, then with secondary antibodies at room temperature for 30 min, next with HRP-labeled streptavidin solution for 30 min, and then finally stained with diaminobenzidine (DAB). For tissue immunofluorescence staining, tissue sections were first deparaffinized with xylene, followed by antigen retrieval using a citrate buffer solution (pH 6.0). After blocking with 10% serum, the samples were incubated overnight with primary antibodies against occludin (ABclonal, A2601, 1:100), ZO-1 (Proteintech, 21773-1-AP, 1:100), and CD31 (Abcam, ab281583), washed three times with PBS, and incubated with the corresponding species-specific secondary antibodies. DAPI was used for nuclear staining. Fluorescence images were captured under a microscope. IHC staining was semi-quantified using an Olympus IX51 microscope (Olympus Corporation, Tokyo, Japan).

The transfer of PKH67-labeled exosomes

PKH67-labeled (Sigma-Aldrich) exosomes derived from MCF7 cells were incubated with diluent C and PKH67 for 5 min at room temperature, followed by termination with serum. After PKH67 labeling, the exosomes were washed three times with PBS to remove excess dye. MCF7 cells were incubated with PKH67-labeled exosomes for 6 h, then washed three times with PBS, and fixed in 4% paraformaldehyde. The cells were subsequently stained with Phalloidin-iFluor 555 (Abcam, ab176756) for 60 min, washed with PBS, and counterstained with DAPI. Finally, images were acquired using the Olympus IX51 microscope (Olympus Corporation).

Immunofluorescence assay and fluorescence in situ hybridization

Endothelial cells cultured on climbing films in 24-well plates were washed with PBS, fixed in 4% paraformaldehyde (Solarbio, P1110) for 20 min at room temperature, and then incubated with primary antibodies against ZO-1 (Proteintech, 21773-1-AP, 1:50) or phalloidin (Abcam, ab176756, 1:1,000) diluted with 1% BSA at 4 °C overnight or room temperature for 50 min. After washing with PBS, the HUVECs were incubated with fluorescently conjugated secondary antibodies (Invitrogen, A-21206, 1:200) for 1 h, washed again, and counterstained with DAPI (Yeasen, 36308ES11, 1:500) for 5 min. Finally, the cells were observed under an Olympus fluorescence microscope.

For FISH, Cy3-labeled circDOCK1-specific (circ0020397) and FAM-labeled miR-1270-specific probes were designed and synthesized by GenePharma (Suzhou, China). The probe signals were determined with the Fluorescent in GenePharma (Suzhou, China) according to the manufacturer's instructions. Images were acquired using a fluorescence microscope (OLYMPUS, IX51).

Cell invasion assay

Transwell inserts with 8-μm pore-size membranes (Corning, 3422, USA) were pre-coated with Matrigel (Corning, 356231, USA) and placed in a 24-well plate (Corning, 3524, USA) containing cell culture medium. A total of 2×10^4 cells were seeded in the upper chamber of the inserts with serum-free medium, while the lower chamber was filled with medium containing 20% serum. The cells were then cultured for 36–48 h at 37 °C with 5% CO_2. Subsequently, the invading cells in the lower chamber were fixed with tissue fixative, stained overnight, and counted under a microscope (OLYMPUS, IX51). At least three random fields per well were selected for counting the number of invading cells and imaging.

TEER, in vitro permeability, and trans-endothelial invasion assays

Endothelial cells monolayers grown on polyethylene terephthalate Transwell filters (0.4 μm, Corning) were analyzed for trans-endothelial electrical resistance (TEER) using a voltohmmeter (Millicell ERS-2, USA). Unit area resistance was calculated following the manufacturer's instructions, with three filters being used for each treatment. For in vitro permeability assays, endothelial cells were treated with exosomes obtained from MCF7 cells for

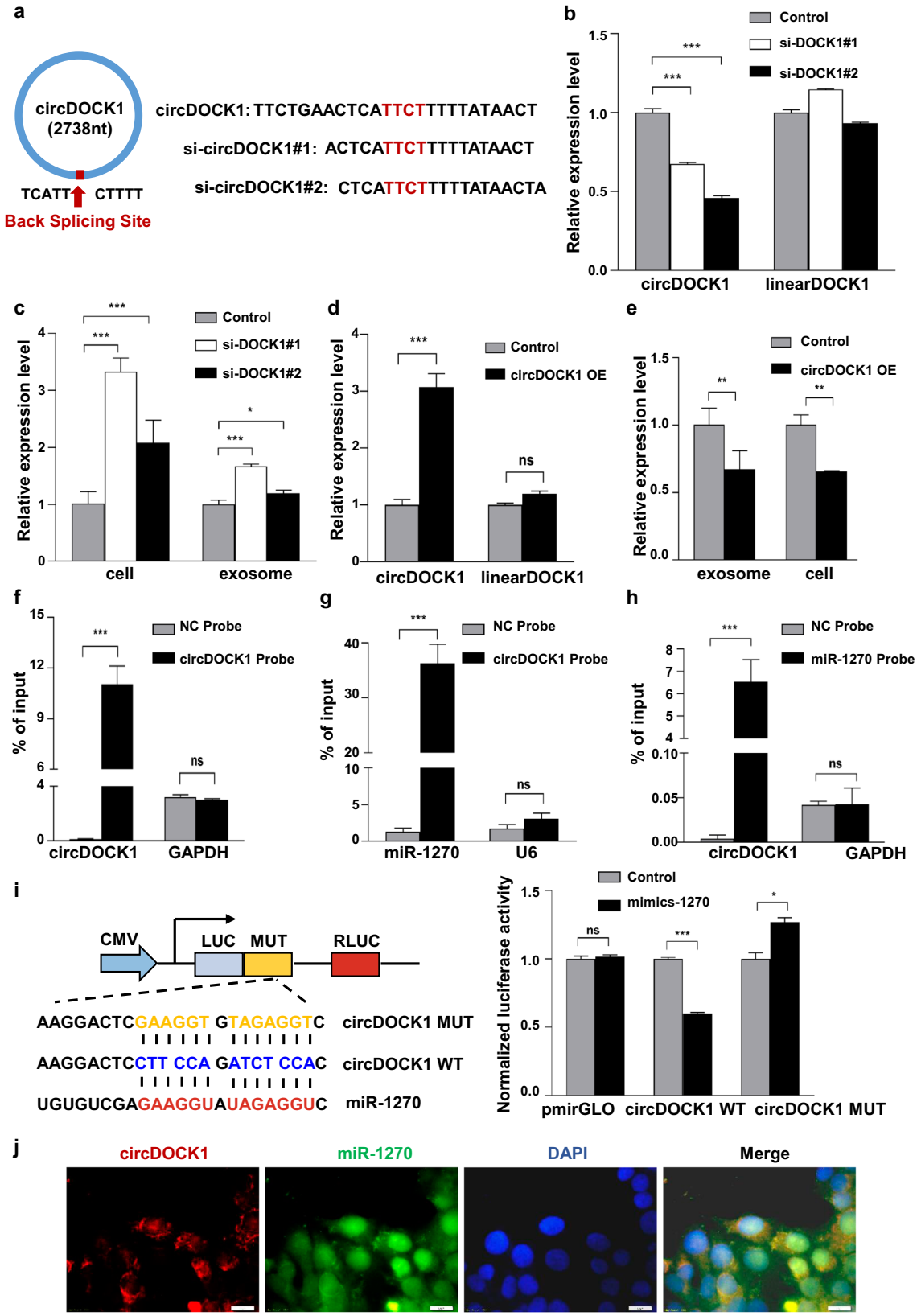

48 hours to form an endothelial monolayer, after which rhodamine B-dextran (Sigma, R9379, Japan) was added to the upper layer of the filters. After 30, 60, and 90 min, the medium in the lower layer of the chamber was collected for measurement of the fluorescence intensity. For the trans-endothelial invasion assay, pre-treated endothelial cells were plated and allowed to reach confluence in the upper chamber of the Transwell filter (8 μm, Corning). A total of 2×10^4 GFP-labeled MCF7 or 2×10^4 GFP-labeled MDA-MB-231 cells were seeded in the Transwell filter. After 48 h, GFP-labeled cells in the lower chamber were observed and counted under a fluorescence microscope.

Fig. 7 | CircDOCK1 suppresses the functions of miR-1270. a The sequences of si-circDOCK1#1 and si-circDOCK1#2, which were designed to target the back-splicing junction site of circDOCK1. **b** qRT-PCR analysis showing that si-circDOCK1#1 and si-circDOCK1#2 specifically target circDOCK1. **c** qRT-PCR analysis of miR-1270 expression in MCF7 cells and exosomes after transfection with si-circDOCK1#1 and si-circDOCK1#2. **d** qRT-PCR analysis of the expression of circDOCK1 and linear DOCK1 in MCF7 cells transfected with Control or circDOCK1 expression constructs. **e** qRT-PCR analysis of miR-1270 expression in MCF7 cells transfected with Control or circDOCK1 expression constructs. **f** Pulldown assay for circDOCK1 using the negative control (NC) probe or the circDOCK1 probe. **g** Pulldown assay for miR-1270 using the NC probe or the circRNA probe. **h** Pulldown assay for circDOCK1 using the NC probe or the miR-1270 probe. **i** Shown are the sequences of wild-type and mutant miR-1270 binding sites that were cloned into the DOCK1 luciferase reporter plasmid. Wild-type (circDOCK1 WT) or mutant (circDOCK1 MUT) luciferase reporter plasmids and miR-1270 mimics or Control were transfected into HEK293T cells, and the relative luciferase activities were analyzed. **j** Fluorescence in situ hybridization (FISH) analysis of the colocalization of circDOCK1 and miR-1270 in MCF7 cells. Scale bars: 10 μm. Data are presented as means ± SEM ($n = 3$ unless otherwise indicated). ns not significant, $^{*}p < 0.05$, $^{**}p < 0.01$, $^{***}p < 0.001$.

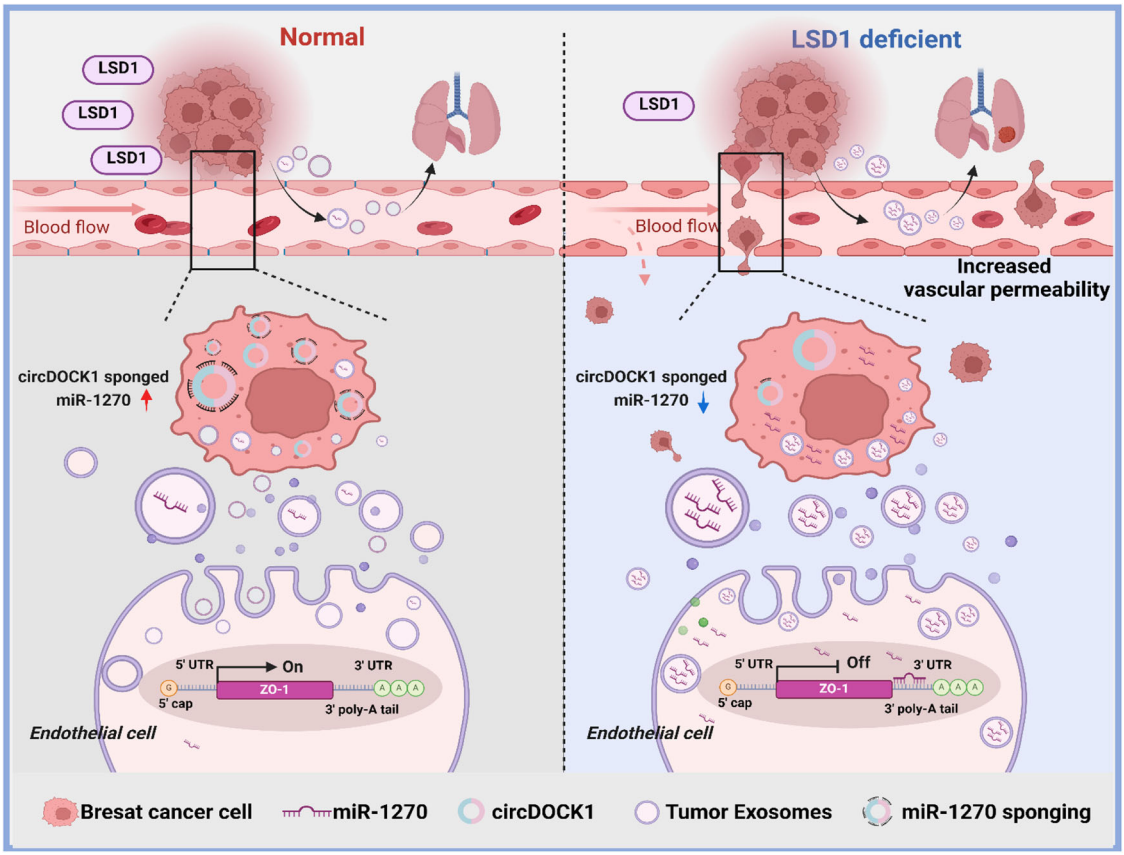

Fig. 8 | The LSD1/circDOCK1/miR-1270 axis regulates the formation of pre-metastatic niches. In breast cancer cells, LSD1 deficiency decreases the expression of circDOCK1, resulting in increased levels of miR-1270 in exosomes. Vascular endothelial cells in distant organs uptake these breast cancer cell-derived exosomes with increased miR-1270 expression, leading to the downregulation of the expression of ZO-1 and other tight junction proteins. Vascular permeability is subsequently enhanced, leading to the formation of pre-metastatic niches and the promotion of lung metastasis. Created with BioRender.com.

Endothelial cells tube formation assay

Endothelial cells were either treated with exosomes or subjected to transfection. For the tube formation assay, pre-cooled 24-well plates were coated with Matrigel and incubated for 60 min in a cell culture incubator. A total of 4×10^4 endothelial cells were seeded in each well and cultured in conditioned medium. Tube formation was monitored and imaged at 12 h intervals using a microscope. The tube-forming ability of the cells was quantified by measuring the cumulative tube length in at least three random fields under a microscope.

Cellular and exosomal sequencing

Analysis of circRNA in cells. Total RNA was extracted using miRNeasy Micro Kit (Cat #217084, Qiagen), and RNA quality was checked using Agilent 4200 TapeStation (Agilent technologies, Santa Clara, CA, US) according to standard procedures. Sequencing libraries were constructed by VAHTS Universal V6 RNA-seq Library Prep Kit for Illumina (Cat #NR604, Vazyme) according to manufacturer's instructions. The sequencing was performed on an Illumina NovaSeq platform (Illumina, San Diego, CA, USA) and analyzed at Shanghai Biochip Co., Ltd., Shanghai, China. Raw data were processed through Seqtk. Next, the clean reads were aligned to the reference genome (GRCh38.104) using HISAT2. The Read Counts of transcripts and ncRNAs were calculated by Stringtie (version:2.1.4). And the expression of mRNA and lncRNA was normalized to FPKM. CIRI2 was utilized for circRNA identification identification and quantification. The identified circRNA was annotated using circBase. The expression of circRNA was normalized to SPRBM.

Analysis of miRNA in exosomes. The exosomes were isolated and total RNA was extracted using exoRNeasy Maxi Kit (#77164, Qiagen). RNA quality was checked using Agilent 4200 TapeStation (Agilent technologies, Santa Clara, CA, US) according to standard procedures. Sequencing libraries were constructed by QIAseq miRNA Library Kit for Illumina (Cat #331505, Qiagen) according to manufacturer's instructions. The sequencing was performed on an Illumina NovaSeq platform (Illumina, San Diego, CA, USA) and analyzed at Shanghai Biochip Co.,

Ltd., Shanghai, China. Raw data were processed with Cutadapt. Next, the clean reads were aligned to the reference Database of miRBase22.1, piRNABank and RfamV14.1 using bowtie-1.3.0. The UMI Counts of small RNA were calculated by perl. And the expression of small RNA was normalized to CPM (Descriptive indicators of gene expression levels). Differential expression miRNA's target genes of mRNA come from miRTarBase database.

RNase R treatment

For RNase R treatment, RNA was incubated with RNase R (Epicentre, RNR07250, USA) for 15 min at 37 °C. Then, total RNA from cells was extracted, and qRT-PCR was used to determine the stability of circ0020397 (circDOCK1).

Bioinformatic analysis

TargetScan, miRDB, and RNA22 were used for predicting miRNA target genes. The functions of the target genes were annotated and KEGG/GO pathway/term enrichment analysis was conducted using KOBAS. MiRDB, miRWalk, TargetScan, and mirDIP were used to predict potential mRNAs that could be targeted by miRNAs. CircBank and CircInteractome were used to predict miRNAs that could be sponged by circ0020397 (circDOCK1).

miRNA pulldown and RNA antisense purification assays

Briefly, MCF7 cells (1×10^7) transfected with miR-1270 probes or control probes were incubated with lysis buffer containing protease and RNase inhibitors. The cell lysate was then incubated with biotin streptavidin-conjugated magnetic beads at 4 °C overnight and, after washing, the immunoprecipitated RNA was purified and analyzed by qRT-PCR to determine circDOCK1 and miR-1270 expression levels. Probe sequences are shown in Supplementary Table 3.

A circDOCK1 biotinylated probe was designed and synthesized by GenePharma (Suzhou, China). For RNA antisense purification assays, the BersinBio RNA Pulldown Kit (BersinBio, Guangzhou, China) was utilized to detect the interactions between circDOCK1 and miR-1270 according to the manufacturer's instructions. Briefy, crosslinked cells were lysed, sonicated, and hybridized with the probes for 4 h at 37 °C. Next, the hybridization mixture was incubated with magnetic beads for 1 h. The bound RNAs and proteins were then washed and purifed for qRT-PCR.

Plasmid construction, RNAi, and cell transfection

Small interfering RNAs (siRNAs) were obtained from Geneseed (Guangzhou, China) and transfected into cells using Lipofectamine 3000 (Invitrogen). The circRNA expression vector Connect circDOCK1 DNA and lentivirus-sh-circDOCK1 were also obtained from Geneseed. The lentiviruses were ultracentrifuged, concentrated, validated, and added to the cell culture medium. After infection, the cells were selected with puromycin (Solarbio) for 1 week, and the surviving cells were continuously cultured as stable mass transfectants.

Statistical analysis

Statistical analysis was performed using GraphPad Prism 8.0.2 (Graph Pad Software). Differences between 2 groups were compared by means of the 2-tailed unpaired Student's t-test. All experiments were performed with at least 3 biological replicates. *P* values are indicated in individual figure legends. Error bars represent SEM.

Data availability

All data generated during this study will be made available on reasonable request. RNA sequencing data sets are deposited at the GEO repository under the accession number GSE264698 and GSE264699.

Received: 23 November 2023; Accepted: 30 October 2024;
Published online: 12 November 2024

References

1. Morgan, E. et al. The global landscape of esophageal squamous cell carcinoma and esophageal adenocarcinoma incidence and mortality in 2020 and projections to 2040: new estimates from GLOBOCAN 2020. *Gastroenterology* **163**, 649–658.e642 (2022).
2. Waks, A. G. & Winer, E. P. Breast cancer treatment: a review. *JAMA* **321**, 288–300 (2019).
3. Harbeck, N. et al. Breast cancer. *Nat. Rev. Dis. Primers* **5**, 66 (2019).
4. Riggio, A. I., Varley, K. E. & Welm, A. L. The lingering mysteries of metastatic recurrence in breast cancer. *Br. J. Cancer* **124**, 13–26 (2021).
5. Nguyen, D. X., Bos, P. D. & Massague, J. Metastasis: from dissemination to organ-specific colonization. *Nat. Rev. Cancer* **9**, 274–284 (2009).
6. Claesson-Welsh, L., Dejana, E. & McDonald, D. M. Permeability of the endothelial barrier: identifying and reconciling controversies. *Trends Mol. Med.* **27**, 314–331 (2021).
7. Liu, Y. & Cao, X. Characteristics and significance of the pre-metastatic niche. *Cancer Cell* **30**, 668–681 (2016).
8. Cao, J. et al. Decylubiquinone suppresses breast cancer growth and metastasis by inhibiting angiogenesis via the ROS/p53/BAI1 signaling pathway. *Angiogenesis* **23**, 325–338 (2020).
9. Varinska, L., Gal, P., Mojzisova, G., Mirossay, L. & Mojzis, J. Soy and breast cancer: focus on angiogenesis. *Int. J. Mol. Sci.* **16**, 11728–11749 (2015).
10. Peinado, H. et al. Pre-metastatic niches: organ-specific homes for metastases. *Nat. Rev. Cancer* **17**, 302–317 (2017).
11. Zeng, Z. et al. Cancer-derived exosomal miR-25-3p promotes pre-metastatic niche formation by inducing vascular permeability and angiogenesis. *Nat. Commun.* **9**, 5395 (2018).
12. Zhou, W. et al. Cancer-secreted miR-105 destroys vascular endothelial barriers to promote metastasis. *Cancer Cell* **25**, 501–515 (2014).
13. Padua, D. et al. TGFbeta primes breast tumors for lung metastasis seeding through angiopoietin-like 4. *Cell* **133**, 66–77 (2008).
14. Rodrigues, G. et al. Tumour exosomal CEMIP protein promotes cancer cell colonization in brain metastasis. *Nat. Cell Biol.* **21**, 1403–1412 (2019).
15. Gurunathan, S., Kang, M. H., Jeyaraj, M., Qasim, M. & Kim, J. H. Review of the isolation, characterization, biological function, and multifarious therapeutic approaches of exosomes. *Cells* **8**, 307 (2019).
16. Xie, Y. et al. The role of exosomal noncoding RNAs in cancer. *Mol. Cancer* **18**, 37 (2019).
17. Zhang, X. et al. Exosomes in cancer: small particle, big player. *J. Hematol. Oncol.* **8**, 83 (2015).
18. Taylor, D. D. & Gercel-Taylor, C. Exosomes/microvesicles: mediators of cancer-associated immunosuppressive microenvironments. *Semin. Immunopathol.* **33**, 441–454, (2011).
19. Falcone, G., Felsani, A. & D'Agnano, I. Signaling by exosomal microRNAs in cancer. *J. Exp. Clin. Cancer Res.* **34**, 32 (2015).
20. Rupaimoole, R. & Slack, F. J. MicroRNA therapeutics: towards a new era for the management of cancer and other diseases. *Nat. Rev. Drug. Discov.* **16**, 203–222 (2017).
21. Li, Y. et al. The SOX17/miR-371-5p/SOX2 axis inhibits EMT, stem cell properties and metastasis in colorectal cancer. *Oncotarget* **6**, 9099–9112 (2015).
22. Harrell, C. R., Jovicic, N., Djonov, V., Arsenijevic, N. & Volarevic, V. Mesenchymal stem cell-derived exosomes and other extracellular vesicles as new remedies in the therapy of inflammatory diseases. *Cells* **8**, 1605 (2019).
23. Conti, I. et al. miRNAs as Influencers of Cell-Cell Communication in Tumor Microenvironment. *Cells* **9**, 220 (2020).
24. Li, X. N. et al. RNA sequencing reveals the expression profiles of circRNA and indicates that circDDX17 acts as a tumor suppressor in colorectal cancer. *J. Exp. Clin. Cancer Res.* **37**, 325 (2018).

25. de Fraipont, F., Gazzeri, S., Cho, W. C. & Eymin, B. Circular RNAs and RNA splice variants as biomarkers for prognosis and therapeutic response in the liquid biopsies of lung cancer patients. *Front. Genet.* **10**, 390 (2019).
26. Jin, C., Wang, A., Liu, L., Wang, G. & Li, G. Hsa_circ_0136666 promotes the proliferation and invasion of colorectal cancer through miR-136/SH2B1 axis. *J. Cell. Physiol.* **234**, 7247–7256 (2019).
27. Lyu, L. et al. Regulatory mechanisms, functions, and clinical significance of CircRNAs in triple-negative breast cancer. *J. Hematol. Oncol.* **14**, 41 (2021).
28. Wang, C. et al. CircRNAs in lung cancer - biogenesis, function and clinical implication. *Cancer Lett* **492**, 106–115 (2020).
29. Salmena, L., Poliseno, L., Tay, Y., Kats, L. & Pandolfi, P. P. A ceRNA hypothesis: the Rosetta Stone of a hidden RNA language? *Cell* **146**, 353–358, (2011).
30. Li, Z. et al. Exon-intron circular RNAs regulate transcription in the nucleus. *Nat. Struct. Mol. Biol.* **22**, 256–264 (2015).
31. Shi, Y. et al. Histone demethylation mediated by the nuclear amine oxidase homolog LSD1. *Cell* **119**, 941–953 (2004).
32. Zheng, Y. C. et al. A systematic review of histone lysine-specific demethylase 1 and its inhibitors. *Med. Res. Rev.* **35**, 1032–1071 (2015).
33. Sukocheva, O. A. et al. The crucial role of epigenetic regulation in breast cancer anti-estrogen resistance: Current findings and future perspectives. *Semin. Cancer Biol.* **82**, 35–59 (2022).
34. Wang, Y. et al. LSD1 is a subunit of the NuRD complex and targets the metastasis programs in breast cancer. *Cell* **138**, 660–672 (2009).
35. Wu, Y. & Zhou, B. P. Epigenetic regulation of LSD1 during mammary carcinogenesis. *Mol. Cell. Oncol.* **1**, e963426 (2014).
36. Choi, H. J. et al. UTX inhibits EMT-induced breast CSC properties by epigenetic repression of EMT genes in cooperation with LSD1 and HDAC1. *EMBO Rep* **16**, 1288–1298 (2015).
37. Li, L. et al. ZNF516 suppresses EGFR by targeting the CtBP/LSD1/CoREST complex to chromatin. *Nat. Commun.* **8**, 691 (2017).
38. Wu, Y. et al. The deubiquitinase USP28 stabilizes LSD1 and confers stem-cell-like traits to breast cancer cells. *Cell Rep* **5**, 224–236 (2013).
39. Cao, C. et al. Functional interaction of histone deacetylase 5 (HDAC5) and lysine-specific demethylase 1 (LSD1) promotes breast cancer progression. *Oncogene* **36**, 133–145 (2017).
40. Zhang, Y. et al. The R251Q mutation of LSD1 promotes invasion and migration of luminal breast cancer cells. *Int. J. Biol. Macromol.* **164**, 4000–4009 (2020).
41. Liu, Z. et al. Exosomes from LSD1 knockdown breast cancer cells activate osteoclastogenesis and inhibit osteoblastogenesis. *Int. J. Biol. Macromol.* **235**, 123792 (2023).
42. Liu, Z. et al. LSD1 modulates the bone metastasis of breast cancer cells through hnRNPA2B1-mediated sorting of exosomal miRNAs. *Cell Death Discov* **10**, 115 (2024).
43. Oshima, T. et al. Tight junction peptide antagonists enhance neutrophil trans-endothelial chemotaxis. *Life Sci* **73**, 1729–1740 (2003).
44. Hansen, T. B. et al. Natural RNA circles function as efficient microRNA sponges. *Nature* **495**, 384–388 (2013).
45. Dudekula, D. B. et al. CircInteractome: a web tool for exploring circular RNAs and their interacting proteins and microRNAs. *RNA Biol* **13**, 34–42 (2016).
46. Wortzel, I., Dror, S., Kenific, C. M. & Lyden, D. Exosome-mediated metastasis: communication from a distance. *Dev. Cell* **49**, 347–360 (2019).
47. Hu, X. et al. LSD1 suppresses invasion, migration and metastasis of luminal breast cancer cells via activation of GATA3 and repression of TRIM37 expression. *Oncogene* **38**, 7017–7034 (2019).
48. Tellez-Gabriel, M., Knutsen, E. & Perander, M. Current status of circulating tumor cells, circulating tumor DNA, and exosomes in breast cancer liquid biopsies. *Int. J. Mol. Sci.* **21**, 9457 (2020).
49. Di Modica, M. et al. Breast cancer-secreted miR-939 downregulates VE-cadherin and destroys the barrier function of endothelial monolayers. *Cancer Lett* **384**, 94–100 (2017).
50. He, Q. et al. Cancer-secreted exosomal miR-21-5p induces angiogenesis and vascular permeability by targeting KRIT1. *Cell Death Dis* **12**, 576 (2021).
51. Sang, M. et al. Circular RNA ciRS-7 maintains metastatic phenotypes as a ceRNA of miR-1299 to target MMPs. *Mol. Cancer Res.* **16**, 1665–1675 (2018).
52. Chen, B. et al. circEPSTI1 as a prognostic marker and mediator of triple-negative breast cancer progression. *Theranostics* **8**, 4003–4015 (2018).
53. Li, S. et al. CircDOCK1 promotes the tumorigenesis and cisplatin resistance of osteogenic sarcoma via the miR-339-3p/IGF1R axis. *Mol. Cancer* **20**, 161 (2021).

Acknowledgements

This work was supported by Jilin Scientific and Technological Development Program [20230508066RC], Special Project for Health Research Talents of Jilin Province [2022SCZ04], Norman Bethune Program of Jilin University [2022B06], and Innovation and Entrepreneurship Talent Funding Project of Jilin Province [2023QN05].

Author contributions

Conceptualization: Y.Y., Y.W., Y.H., and X.H. Data curation: Y.Y., R.Q., Y.S., and P.A. Formal analysis: Y.Y., H.G., and Y.D. Methodology: Y.Y., R.Q., H.G., Y.D., and P.A. Validation: Y.Y., R.Q., H.G., Y.D., Y.S., B.X., Z.L., and N.Z. Visualization; Y.Y., and R.Q. Writing - original draft: Y.Y. Writing - review and editing: Y.Y., Y.W., and X.H. Funding acquisition: X.H. Project administration: Y.W., and X.H. Supervision: X.H. All authors have read and agreed to the published version of the manuscript.

Competing interests

The authors declare no competing interests.

Additional information

Supplementary information The online version contains supplementary material available at https://doi.org/10.1038/s41698-024-00751-2.

Correspondence and requests for materials should be addressed to Xin Hu.